Energy enhancement and chaos control in microelectromechanical systems

Kwangho Park,[1] Qingfei Chen,[1] and Ying-Cheng Lai[1,2]
[1]*Department of Electrical Engineering, Arizona State University, Tempe, Arizona 85287, USA*
[2]*Department of Physics and Astronomy, Arizona State University, Tempe, Arizona 85287, USA*
(Received 20 April 2007; revised manuscript received 19 October 2007; published 12 February 2008)

For a resonator in an electrostatic microelectromechanical system (MEMS), nonlinear coupling between applied electrostatic force and the mechanical motion of the resonator can lead to chaotic oscillations. Better performance of the device can be achieved when the oscillations are periodic with large amplitude. We investigate the nonlinear dynamics of a system of deformable doubly clamped beam, which is the core in many MEMS resonators, and propose a control strategy to convert chaos into periodic motions with enhanced output energy. Our study suggests that chaos control can lead to energy enhancement and consequently high performance of MEM devices.

DOI: 10.1103/PhysRevE.77.026210 PACS number(s): 05.45.Pq, 85.85.+j

With the advances of nanoscience and nanotechnology, interest in the nonlinear dynamics of small-scale systems has appeared [1–3]. Take, for example, nanosized resonators [4] that are capable of operating in extremely high frequency ranges. However, at smaller sizes, the output energies of such resonators are typically weaker and the effect of nonlinearity becomes severe. The latter is so because some essential components in a resonator, such as a cantilever beam, can behave nonlinearly at even modest amplitude, leading, for instance, to chaotic dynamics. While there have been many advances in the fundamentals of nonlinear dynamics and chaos in the past three decades, little has been done to extend the research to small-scale devices, which have become increasingly important in many areas of science and engineering.

In certain applications such as microfluid mixers [5] and communication [6,7], chaos is desirable. However, for typical applications of high-frequency resonators, chaos is considered as undesirable. One wishes to control chaos to generate periodic dynamics and obtain strong output energy even at very small sizes. In this paper, we consider a paradigmatic class of small-size devices, namely, microelectromechanical systems (MEMS) with a resonant beam, and demonstrate the ubiquity of chaos and devise a feasible strategy to control chaos and more importantly, to enhance the output energy of the MEMS resonator. Mathematically, such a resonator is described by a nonlinear partial differential equation with sophisticated boundary conditions arising from the electrophysics and mechanics of the device. While our chaos control and energy enhancement strategy is not sophisticated, the demonstration is that it is effective in MEMS resonator, a spatiotemporal dynamical system of high phase-space dimension, is remarkable. We provide a physical theory to explain the phenomenon of energy enhancement as a result of chaos control. To our knowledge, prior to this work there has been little effort to address the problem of energy enhancement in small-scale devices, an important topic in nanoscience and engineering. We expect our result to find broad applications.

The resonating behavior of a deformable, doubly clamped beam in MEMS has attracted a great deal of recent attention [1,2,4,5,8–13]. A doubly clamped flat beam over the ground plate in MEMS has a simple structure but shows rich dynamical behaviors when an external voltage is applied [1]. The applied voltage generates a potential difference between the two conductors, the beam and the ground plate, leading to electrostatic charges on their surfaces. Due to the change in the distance between the conductors, the charge distributions can change accordingly, inducing an interacting force between the conductors. In particular, when a dc voltage is applied to MEMS, the induced force causes the beam to be deformed toward the ground plate. If the voltage exceeds a certain dc pull-in voltage, the center of the beam can move and even touch to the ground plate. If the applied dc voltage is near but less than the pull-in voltage, the force becomes nonlinear with respect to the displacement of the beam, leading to nonlinear dynamics. In this case, when an ac voltage is applied, the nonlinear interaction can lead to a rich variety of oscillatory behaviors. Typically, the beam oscillates periodically for small ac amplitude but chaos can arise through a cascade of periodic-doubling bifurcations as the ac voltage amplitude is increased.

To be concrete, we consider a doubly clamped beam, as shown in Fig. 1. The general equation governing the time-dependent deformation of the beam in the presence of an electrical field can be obtained by considering the following standard, two-dimensional nonlinear analysis of the microstructure [11]:

$$\rho\ddot{\mathbf{u}} = \nabla \cdot (\mathbf{FS}) \text{ in } \Omega, \tag{1}$$

$$\mathbf{u} = \mathbf{G} \text{ on } \Gamma, \tag{2}$$

$$\mathbf{P} \cdot \mathbf{N} = \mathbf{H} \text{ on } \Gamma, \tag{3}$$

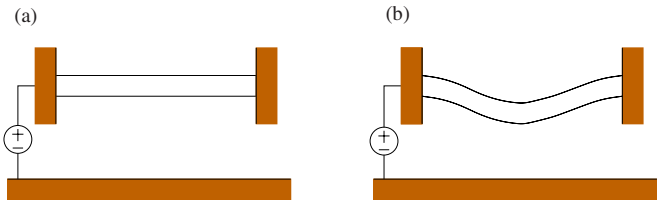

FIG. 1. (Color online) Doubly clamped beam over a ground plate. (a), (b) Nondeformed and deformed structure before and after a voltage is applied.

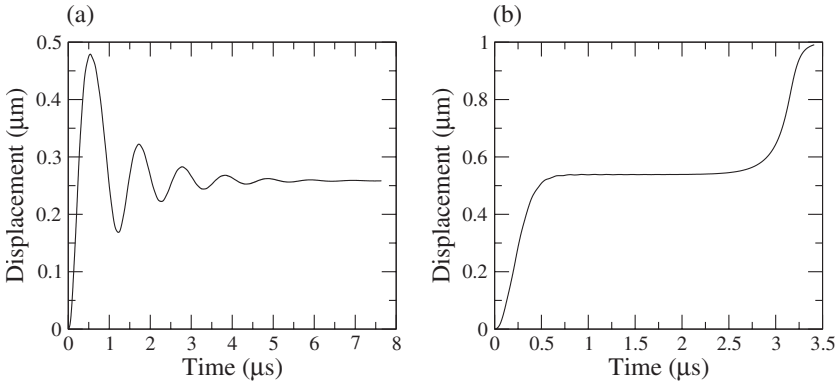

FIG. 2. Under dc voltage, displacement of the beam center vs time. (a) For $V_{dc}=68.0$ V, the beam reaches a steady state after a transient. (b) For $V_{dc}=69.0$ V, beam center starts bending as soon as a dc voltage is applied. It remains at about 4.4 μm from the ground plate for some time and then moves relatively quickly to touch and to stick to the ground plate.

$$\mathbf{u}|_{t=0} = \mathbf{G}_0 \text{ in } \Omega, \tag{4}$$

$$\dot{\mathbf{u}}|_{t=0} = \mathbf{V}_0 \text{ in } \Omega, \tag{5}$$

where $\mathbf{u}$, $\dot{\mathbf{u}}$, and $\ddot{\mathbf{u}}$ are the displacement, velocity, and acceleration vectors, respectively; ρ, $\mathbf{F}$, and $\mathbf{S}$ are the material density in the initial configuration, the deformation gradient, and the second Piola-Kirchhoff stress, respectively; $\mathbf{N}$ is the unit outward normal vector in the initial configuration and $\mathbf{G}$ is the prescribed displacement; $\mathbf{G}_0$ and $\mathbf{V}_0$ are the initial displacement and velocity, respectively; $\mathbf{P}$ is the first Piola-Kirchhoff stress tensor and $\mathbf{H}$ is the electrostatic pressure acting on the surface of the structures; Ω and Γ denote domain and boundary, respectively; $\mathbf{H}$ is a function of the air damping pressure p due to the thin air (or fluid) film squeezed between the moving plate and the ground plate. The following Reynold's squeeze film equation can be used to compute the pressure, which can be derived from the Navier-Stokes equation under the assumptions that the inertial terms are negligible compared to viscous terms, there is no pressure gradient through the film, and the flow in the direction perpendicular to the plates is negligible [12]:

$$\frac{\partial}{\partial x}\left(g^3\frac{\partial p}{\partial x}\right) + \frac{\partial}{\partial y}\left(g^3\frac{\partial p}{\partial y}\right) = 12\eta\frac{\partial g}{\partial t}, \tag{6}$$

where x and y are the coordinates along and perpendicular to the plate, respectively, η is the air viscosity, g is the film thickness, and the density of air is assumed to be constant.

For the beam structure considered, Eqs. (1)–(5) can be simplified to yield [12]

$$EI\frac{\partial^4 u}{\partial x^4} + \rho A\frac{\partial^2 u}{\partial t^2} = f_E - f_A, \tag{7}$$

with the boundary conditions imposed on the displacements and their slopes at both fixed ends

$$u(0,t) = u(L,t) = 0,$$

$$\frac{\partial u(0,t)}{\partial x} = \frac{\partial u(L,t)}{\partial x} = 0. \tag{8}$$

In Eqs. (7) and (8), $u(x,t)$ denotes the downward deflection of the beam, E is the Young's modulus, ρ is the material density, $A=wh$ (width $\times$ thickness) and $I=wh^3/12$ are the area and moment of inertia of the beam's rectangular cross section, respectively, f_A is the mechanical load from the squeezed air film between the beam and the ground plate, and f_E is the electrostatic force per unit length of the beam which is given by $f_E=\epsilon_0 V^2 w/2g^2$. In this expression, ϵ_0 is the permittivity of free space and $V(t)=V_{dc}+V_{ac}\cos(2\pi ft)$ is the voltage between the beam and the ground plate separated by the gap $g(x,t)=g_0-u(x,t)$, and f and g_0 denote frequency and the initial gap, respectively.

Since Eq. (6) is linear in p, the pressure can be replaced by the pressure variation $\tilde{p}=p-p_a$, where p_a is ambient atmospheric pressure. Applying the boundary condition $\tilde{p}=0$ to the beam edges and using the assumption that the pressure is a separable function of x and y, i.e., $\tilde{p}(x,y,t)=\tilde{P}(x,t)(1-4y^2/w^2)$ [14], we obtain

$$2\hat{g}^2\left(\frac{g_0}{L}\right)^2\frac{\partial\hat{g}}{\partial\hat{x}}\frac{\partial\tilde{P}}{\partial\hat{x}} + \frac{2}{3}\hat{g}^3\left(\frac{g_0}{L}\right)^2\frac{\partial^2\tilde{P}}{\partial\hat{x}^2} - 8\frac{\hat{g}^3}{\hat{w}^2}\tilde{P} = 12\eta\frac{\partial\hat{g}}{\partial t}, \tag{9}$$

where $g=g(x,t)$ is assumed to be independent of y and some nondimensionalized quantities are used: $\hat{x}=x/L$ (L: beam length), $\hat{g}=g/g_0$, and $\hat{w}=w/g_0$. Since generally $g_0 \ll L$ for a doubly clamped beam in MEMS, Eq. (9) can be further simplified by ignoring terms of the order of $(g_0/L)^2$. The pressure is thus obtained as $\tilde{P}(x,t)=(3/2)(\eta w^2/g^3)(\partial g/\partial t)$. The force per unit length owing to the pressure of the squeezed air film, f_A, is obtained by integrating $\tilde{p}(x,y,t)$ with respect to y across the width of the beam. We obtain

$$f_A = -\int_{-w/2}^{w/2}\tilde{P}(x,t)\left(1-\frac{4y^2}{w^2}\right)dy = -\frac{\eta w^3}{g^3}\frac{\partial g}{\partial t}. \tag{10}$$

With the above modeling analysis, the numerical simulation of the device whose dynamics are described by Eq. (7) can be carried out. The parameters of our simulations are given as follows: beam length $L=300$ μm, width $w=10$ μm, thickness $h=1$ μm, the initial gap $g_0=1$ μm, Young's modulus $E=169$ GPa, density $\rho=2330$ kg/m^3, Poisson's ratio $\nu=0.3$, and the viscosity $\eta=1.82\times10^{-5}$ kg/ms for air. With these settings, the governing equation of the doubly clamped beam, Eq. (7), is solved here by a standard finite element method [15]. A total of six elements are employed for numerical analysis. When the applied dc voltage is smaller than the dc pull-in voltage $V_{dc}\approx 69.0$ V, the beam oscillates initially but after a transient it reaches a steady deformed state due to fluid damping [Fig. 2(a)]. At

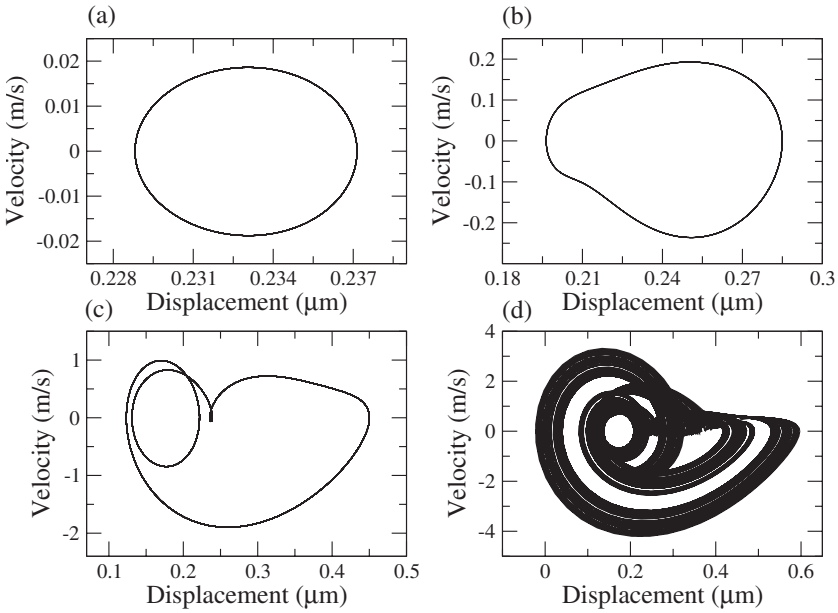

FIG. 3. Under an ac voltage, phase-space trajectory characterizing the dynamics of the beam center. (a),(b) Period-1 behavior for $V_{ac}=0.3$ V and $V_{ac}=3.0$ V, respectively, (c) a period-3 state for $V_{ac}=6.4$ V, and (d) chaos for $V_{ac}=6.7285$ V cascade of period-doubling bifurcations.

$V_{dc}=69.0$ V, a dynamical pull-in of the beam occurs, as shown in Fig. 2(b). To study the effect of ac voltage on the beam dynamics, we fix $V_{dc}=66.2$ V and vary the amplitude of the applied ac voltage from zero to $V_{ac}=6.735$ V, above which the phenomenon of pull-in due to ac voltage occurs. To visualize the dynamics, we focus on the center point of the beam and define a dynamical trajectory to be the path traversed by the center point in the phase space (position and velocity). For small ac voltage, the trajectory is a period-1 orbit, as shown in Figs. 3(a) and 3(b) for $f=714$ KHz. As the ac voltage is increased, period-doubling bifurcations occurs, leading eventually to chaotic oscillations [16], as shown in Figs. 3(c) and 3(d).

We now demonstrate that controlling chaos [17] and enhancing energy output can be accomplished at the same time, namely, when chaos is converted into some periodic motion, the output energy of MEMS resonator can be increased. This is remarkable considering that in the literature, a commonly practiced method to increase the energy of the MEMS resonator is to use an array of identical cantilever beams [9,10,18], but the size of such an array system is usually much larger than that of a single cantilever beam. In order to control chaos in a single doubly clamped beam [19], we propose a controlling perturbation of the form $f_C=C_m\delta(x,x_c)\{\bar{u}(x,t)-u(x,t)\}$, where $\bar{u}(x,t)=\beta[\cos(2\pi ft/n)+1]$, C_m and n are parameters, x_c denotes the beam center, and $\delta(x,x_c)$ is a delta function satisfying the condition: $\delta(x,x_c)=1$ if $x=x_c$ and $\delta(x,x_c)=0$ if $x\neq x_c$. The frequency, $2\pi ft/n$, we use for chaos control is exactly the same as that of the applied voltage $V(t)$ in the system for $n=1$. As our numerical implementation demonstrates, time-delayed feedback control appears not necessary to convert chaos in the MEM beam dynamics into periodic motions.

The system under the control can be written as

$$EI\frac{\partial^4 u}{\partial x^4}+\rho A\frac{\partial^2 u}{\partial t^2}=f_E-f_A+f_C. \tag{11}$$

To be concrete, we investigate Eq. (11) for $n=2$ and $\beta=0.25$, 0.2, and 0.08. Under the control perturbation, the beam shows a transition from chaotic to periodic oscillations with the increase of C_m for all values of β that we have considered. The amplitude of periodic oscillations has different values depending on β and C_m. A numerical bifurcation analysis indicates that, as C_m is increased through a small critical value, the dynamics of the beam is robustly periodic. Figure 4(a) shows a chaotic time series for the displacement of the beam center for $C_m=0$ and $f=500$ KHz. The corresponding phase-space trajectory is shown in Fig. 4(c). A controlled periodic time series is shown in Fig. 4(b) for $C_m=11.1\times10^{-6}$. Figures 4(d)–4(f) show, for three values of C_m in increasing order, controlled periodic trajectories. We find that the amplitude of the beam oscillation increases with the magnitude of the control, while the beam dynamics remains to be periodic. This means that, controlling chaos, besides converting the undesirable chaotic behavior into periodic motion, can bring in an extra advantage: the output energy of the MEMS resonator can be enhanced.

In traditional chaos control, the control perturbation vanishes when periodic motion is achieved. In our scheme, the control force responds to the displacement of the MEM beam. As a result, when the beam is controlled so that periodic motion is achieved, control becomes periodic, too. This is needed for energy enhancement through the mechanism of resonance. Figures 5(a)–5(d) show time series for the displacement of the beam center and the control term $f_C(t)$ for $n=2$. When the control term is absent, i.e., $f_C(t)=0$, the displacement shows a chaotic behavior, but when the term is turned on, both the displacement and control perturbation become periodic.

We now give a heuristic explanation to the phenomenon of energy enhancement together with chaos control. A recent work has shown that some dynamical features of our realistic MEMS resonator with a microcantilever beam can be captured by the dynamics of a simple damped oscillator [1] described by $m\ddot{x}+b\dot{x}+kx=F_E$, where m, b, and k are the mass, the damping coefficient, and the harmonic spring constant, respectively. The nonlinear driving force $F_E=\epsilon wLV^2/\{2(g_0-x)^2\}$ is the static electrical force, where g_0 is

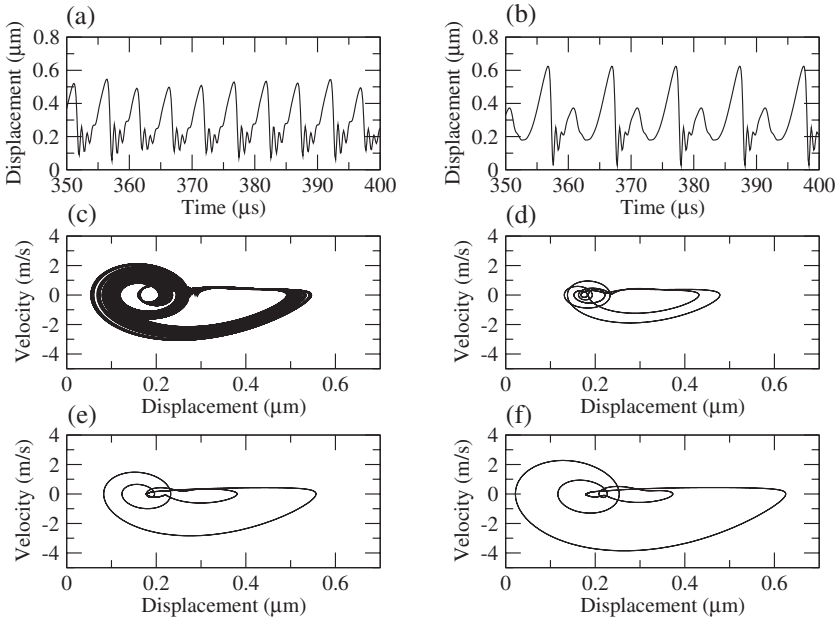

FIG. 4. For $V_{dc}=66.2$ V and $V_{ac}=6.535$ V, (a),(c) uncontrolled chaotic time series and trajectory for $C_m=0$, (b) controlled periodic time series for $C_m=11.1\times10^{-6}$, and (d)–(f) controlled periodic trajectories for $C_m=2\times10^{-6}$, 10×10^{-6}, and 11.1×10^{-6}, respectively.

the gap in the undeformed state between the microstructure and the ground electrode, wL is the area of the microstructure surface facing the ground electrode and $V=V_{dc}+V_{ac}\exp(i2\pi ft)$ is the applied voltage. The equation for the damped oscillator can be rearranged by using $y=g_0-x$. We obtain

$$-y^2m\ddot{y}-y^2b\dot{y}+y^2k(g_0-y)=\epsilon wLV^2/2$$
$$=A_0+A_1\exp(i2\pi ft)+A_2\exp(i4\pi ft),$$

where $A_0=\epsilon wLV_{dc}^2$, $A_1=\epsilon wLV_{dc}V_{ac}$, and $A_2=\epsilon wLV_{ac}^2/2$. The displacement variable $y(t)$ can be represented by a Fourier series: $y=\Sigma_{P=0}^{\infty}Y_P\exp(iP2\pi ft)$. The findings in Ref. [1] reveal that the value of Y_M peaks at $f=f_0/M$, where $f_0=\sqrt{k/m}/(2\pi)$ is the resonant frequency, leading to maximum of the ratio Y_M/Y_1 at that frequency. In particular, the first amplitude Y_1 in the series is usually much larger at the resonance frequency than the rest of the amplitudes, as Y_M decreases rapidly with M.

In the presence of control, the simple oscillator model becomes $m\ddot{x}+b\dot{x}+kx=F_E+F_C$, where $F_C=C_m[\beta\{\exp(i2\pi ft/n)+1\}-x]$ is the control force. A detailed analysis yields analytic expressions for Y_P. For instance, Y_0 and Y_1 for $n=1$ are given by $Y_0^3-g_0Y_0^2+\tilde{A}_0/\tilde{k}=0$ and $Y_1=\tilde{A}_1/(G_0+G_1)$, where $\tilde{A}_0=A_0+\beta C_mY_0^2$, $\tilde{k}=k+C_m$, $\tilde{A}_1=A_1+\beta C_mY_0^2$, $G_0=mY_0^2\omega^2-3kY_0^2+2kg_0Y_0-ibY_0^2\omega$, and $G_1=-2\beta C_mY_0-3\beta C_mY_0^2+2g_0\beta C_mY_0$. Since $k\gg C_m$, $g_0\gg\tilde{A}_0/\tilde{k}$,

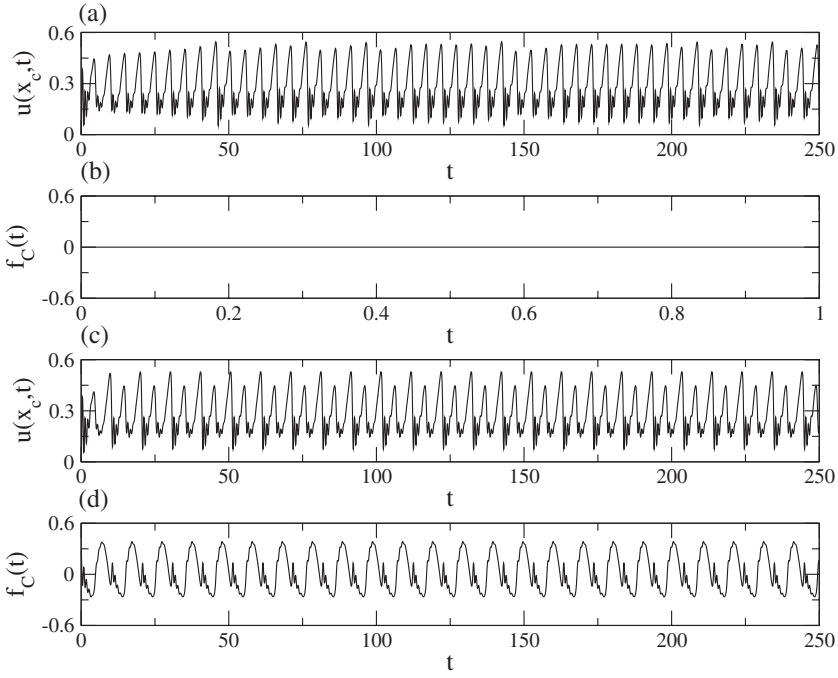

FIG. 5. Time series of the displacement $u(x_c,t)$ for $V_{dc}=66.2$ V and $V_{ac}=6.535$ V (a) when the control term $f_C(t)$ is turned off and (c) when it is turned on. Time series of $f_C(t)$ (b) when it is turned off and (d) when it is turned on.

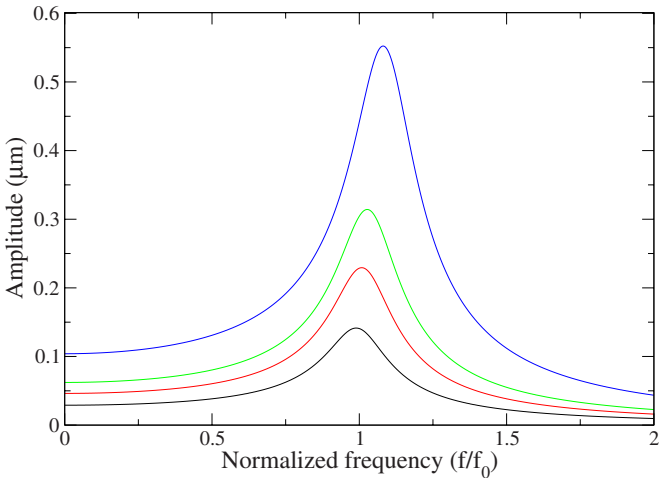

FIG. 6. (Color online) The plot of Y_1 vs the normalized frequency for $C_m=0$, 0.2×10^{-6}, 0.3×10^{-6}, and 0.5×10^{-6} from bottom to top. The locations of the maxima on the frequency axis in $Y_1(f/f_0)$ shift toward the right with C_m. We see that Y_1 increases with C_m, as predicted by our theory.

and $Y_0 \gg Y_0^2$ in the system considered, we obtain approximately $Y_0 \simeq g_0$ and $Y_1 \simeq (A_1+\beta C_m Y_0^2)/(G_0-2\beta C_m Y_0\}$, which increases with C_m. The resonance frequency of the system becomes $f_0'=\sqrt{(k+C_m)/m}/(2\pi)$, which is greater than that in the original system with $C_m=0$. The locations of the maxima on the frequency axis in the coefficients $Y_M(f)$ then shift toward the right. Since the amplitude of Y_1 is much larger than Y_M $(M \geqslant 2)$, it dominates the oscillating amplitude. Controlling chaos enhances Y_1, which means the energy output of the controlled system is increased. Figure 6 shows an example of the increase of Y_1 with C_m in the plot of Y_1 versus f/f_0, where the parameter values are $m=\rho whL=1.78\times10^{-12}$ kg, $b=2.832\times10^{-6}$ Ns/m, $k=105.625$ N/m, $V_{dc}=66.2$ V, and $V_{ac}=6.535$ V.

In conclusion, we have investigated the nonlinear dynamics of a doubly clamped beam on micrometer scales, under applied voltages. Such beam systems are the central component of many state-of-art MEMS resonators. We have found that chaos can occur commonly in such systems and we propose an effective strategy to control chaos and, at the same time, to enhance the oscillating amplitude of the beam while keeping the dynamics periodic. A feasible way to verify our results experimentally is as follows: Fabricate a small vertical thin finger (beam) at the center of a doubly clamped beam and then apply a driving force by electrostatic comb drive to the finger beam, where the applied electrostatic force is determined by the voltage difference between the comb drive electrode and the clamped beam. With a detecting device such as optical microprobe [21], one can get information about the center displacement of the clamped beam as a function of time, which makes it possible for a specially designed circuit to supply the electrostatic comb drive with a proper voltage to realize the feedback force f_C.

We remark that there have been recent studies of the effects of nonlinearity on parametric resonance in a micromachined oscillator, where nonlinearity can change the stability characteristics of parametric resonance significantly [20]. It has been shown that some of the nonlinear effects can be used as a method to increase the device output energy. These studies and ours represent encouraging examples where the principles of nonlinear dynamics can be used for enhancing the performance of small-sized devices [20]. Such devices are the core of intense current research in nanoscience and nanotechnology, where we expect the role of nonlinear dynamics to become increasingly essential.

This work was supported by AFOSR under Grant No. FA9550-06-1-0024.

[1] S. K. De and N. R. Aluru, Phys. Rev. Lett. **94**, 204101 (2005); J. Microelectromech. Syst. **15**, 355 (2006).
[2] J. D. Posner and J. G. Santiago, J. Fluid Mech. **555**, 1 (2006).
[3] M. Yousefi, Y. Barbarin, S. Beri, E. A. J. M. Bente, M. K. Smit, R. Nötzel, and D. Lenstra, Phys. Rev. Lett. **98**, 044101 (2007).
[4] H. G. Craighead, Science **290**, 1532 (2000); X. M. H. Huang, C. A. Zorman, M. Mehregany, and M. L. Roukes, Nature (London) **321**, 496 (2003); H. B. Peng, C. W. Chang, S. Aloni, T. D. Yuzvinsky, and A. Zettl, Phys. Rev. Lett. **97**, 087203 (2006); S.-B. Shim, M. Imboden, and P. Mohanty, Science **316**, 95 (2007).
[5] H. Lin, B. D. Storey, M. H. Oddy, C. H. Chen, and J. G. Santiago, Phys. Fluids **16**, 1922 (2004).
[6] C. T.-C. Nguyen, Nanotechnology **1**, 452 (2003).
[7] A.-C. Wong and C. T.-C. Nguyen, J. Microelectromech. Syst. **13**, 100 (2004).
[8] K. Pyragas, Phys. Lett. A **170**, 421 (1992); K. Pyragas and A. Tamaševičius, *ibid.* **180**, 99 (1993); Y. C. Kouomou and P. Woafo, Phys. Rev. E **66**, 036205 (2002).
[9] E. Buks and M. L. Roukes, J. Microelectromech. Syst. **11**, 802 (2002).
[10] M. C. Cross, A. Zumdieck, R. Lifshitz, and J. L. Rogers, Phys. Rev. Lett. **93**, 224101 (2004).
[11] S. K. De and N. R. Aluru, J. Microelectromech. Syst. **13**, 737 (2004).
[12] S. Krylov and R. Maimon, J. Vibr. Acoust. **126**, 332 (2004).
[13] V. Kaajakari, T. Mattila, A. Oja, and H. Seppä, J. Microelectromech. Syst. **13**, 715 (2004).
[14] B. McCarthy, G. G. Adams, and N. E. McGruer, J. Microelectromech. Syst. **11**, 276 (2002).
[15] T. J. R. Hughes, *The Finite Element Method, Linear Static and Dynamic Finite Element Analysis* (Prentice-Hall, Englewood Cliffs, NJ, 1987).
[16] Similar dynamical behaviors were found recently for a fixed-fixed beam by De *et al.* [1].
[17] M. Ashhab, M. V. Salapaka, M. Dahleh, and I. Mezić, Automatica **35**, 1663 (1999); Nonlinear Dyn. **20**, 197 (1999); K. Yamasue and T. Hikihara, Rev. Sci. Instrum. **77**, 053703 (2006); Y. Fang, D. Dawson, M. Feemster, and N. Jalili, *Pro-*

ceedings of 2002 ASME International Mechanical Engineering Congress and Exposition (ASME, New York, 2002), p. 33539.

[18] M. Sato, B. E. Hubbard, A. J. Sievers, B. Ilic, D. A. Czaplewski, and H. G. Craighead, Phys. Rev. Lett. **90**, 044102 (2003).

[19] E. Ott, C. Grebogi, and J. A. Yorke, Phys. Rev. Lett. **64**, 1196 (1990).

[20] W. Zhang, R. Baskaran, and K. L. Turner, Sens. Actuators, A **102**, 139 (2002); Appl. Phys. Lett. **82**, 130 (2003); W. Zhang and K. L. Turner, Sens. Actuators, A **122**, 23 (2005).

[21] J. M. Dawson, L. Wang, P. Famouri, and L. A. Hornak, Opt. Lett. **28**, 1263 (2003).